

Aerodynamic Effects of Leading-Edge Flap Angle on NACA 4412 Airfoil Performance at Low Reynolds Numbers: A CFD Investigation

Sayed Tanvir Ahmed,^{a)} Ratul Das,^{b)} Tripta Sarker,^{c)} and Mahadi Hasan Shanto^{d)}

Department of Mechanical Engineering, Shahjalal University of Science and Technology, Sylhet-3114, Bangladesh.

^{a)}Corresponding author: sytanvir.mech@gmail.com

^{b)}ratuldas.9052@gmail.com

^{c)}triptasarker@gmail.com

^{d)}mahadishanto27@gmail.com

Abstract. In this contemporary era, the significance of wind energy is increasing enormously to address the energy crisis. The aerodynamic efficiency of a wind turbine is heavily influenced by the blade's airfoil profile and selecting an appropriate profile is essential. A numerical (CFD) based investigation is conducted on the NACA 4412 airfoil profile by modifying the leading-edge flap angle in order to assess the impact on the aerodynamic performance of wind turbine blades. The governing equations, incorporating the Spalart-Allmaras turbulence model, were solved using the commercial software ANSYS FLUENT CFD algorithm, and structured grid was constructed using ANSYS ICEM CFD. In this investigation, the leading-edge flap angle (at 20% chord) of NACA 4412 was varied with a 2° interval between 8° up flap to 8° down flap, for a total of nine airfoil configurations. The Reynolds number (Re) used in this investigation was 0.3 million whereas the angle of attack ranged from 0° to 20°, with 1° increments. The research examined and reported the impact of varying leading-edge flap angles on the lift coefficient (C_L), drag coefficient (C_D), and lift-to-drag ratio (C_L/C_D) at different angles of attack. In order to comprehend the aerodynamic properties and flow physics, the influence of flap angles on the velocity and pressure distributions surrounding the airfoil was examined and visually illustrated. The 8° down flap configuration exhibited the highest aerodynamics performance, achieved by a maximum lift-to-drag ratio (C_L/C_D) enhancement of 10.7% compared to the NACA 4412 base profile.

INTRODUCTION

In this day and age, there are significant factors that have prompted global attention towards renewable energy. One of the most predominant reasons is that the quantity of fossil fuels is reducing enormously for the higher energy demand. Among most of the renewable energy sources such as geothermal energy, solar energy, and ocean energy, the viability of wind energy is the most. There are predominately two types of wind turbines: one is the horizontal axis wind turbine (HAWT) and the other is the vertical axis wind turbine (VAWT).

Significant technological advancements in vertical axis wind turbine (VAWT) systems attest to the wind industry's substantial global expansion [1]. In spite of the fact that the installation rate of the wind turbine is adequate in Europe and the USA, this rate is inadequate in the Indian Subcontinent. However, this rate has been increasing in recent years. Especially, in Bangladesh, the utilization of wind energy rose from 80 MW in 2021 to 150 MW in 2022 [2]. It is expected that the Bangladesh government will give more priority to wind energy in order to face the energy crisis. Intriguingly, China generates 7.5% of its total electricity, which indicates a significant number. Additionally, it has been noticed in recent years that almost every government around the globe is giving priority to wind energy. In order to obtain effective output from a wind turbine, the installation and maintenance of the wind turbine should be faultless. A wind turbine's potential to produce power might be lost to a larger extent as a result of improper installation.

Unfortunately, the overall performance of the wind turbine is subpar because the horizontal axis wind turbine's efficiency is only 59.3% [3]. The performance of a wind turbine blade mostly relies on the lift and drag force which are highly dependent on the cross-section shape and size of the wind turbine blade also called airfoil [4]. To achieve optimal aerodynamic performance of the airfoil, it is desirable to have a larger lift force and a smaller drag force [5]. A study on various airfoils utilizing different Reynolds numbers suggested that the Reynolds number has a strong impact on determining the performance of airfoils [6]. Different types of airfoils have already been invented, though scientists are continuously trying to invent the most highly performed airfoil. Among different airfoil series, the NACA airfoil series is renowned because of some potential causes. NACA airfoils are utilized both in the wind turbine and aircraft and the cross-section, such as the NACA 4412 airfoil, can be rapidly generated [7], [8]. A comparative study was done on a symmetrical airfoil named NACA 0012 and an asymmetrical airfoil named NACA 4412, which indicate that the asymmetrical airfoils generate relatively better lift [9]. Another study was done on the CQU-A airfoil series and these

airfoils are highly viable for the wind turbine blade [10]. An experimental study performed by Şahin & Acir [11] on NACA 0015 found the drag and lift coefficient increase with the attack angle. Using a blade element-momentum theory a study was conducted by Migloire [12] to examine the performance of NACA 6-series and NACA 4-digit airfoils for Darrieus wind turbines. Moreover, a study in 2021 compared 9 airfoils from 3 different airfoil families; these families are NACA, FX, and S. The results indicate that FX 60-157, and S 4412 provide the maximum lift coefficient at 12° angle of attack among nine airfoils [13]. Computational fluid dynamics (CFD) is a viable alternative for predicting aerodynamic characteristics since time and cost are associated in experimental studies [14].

In this study, The NACA 4412 was chosen for the analysis by varying leading edge flap mainly because it's a potential airfoil for use in wind turbines which can yield good performance. The objectives of this paper are as follows:

1. To investigate the effect of the leading-edge flap angle of NACA 4412 on lift coefficients, drag coefficients, and drag-to-lift ratio with the angle of attack.
2. To achieve the best leading-edge configuration of NACA 4412 to implement to wind turbine blade.

The lift coefficient, drag coefficient, and lift-to-drag ratio were initially analyzed for 0° to 20° angle of attack (AOA) in this study and presented graphically. Finally, pressure contours and velocity contours were investigated and illustrated pictorially to understand the overall characteristics and flow physics.

NUMERICAL INVESTIGATION

An object in the air encounters both lift and drag forces. The lift and drag coefficients are derived from the lift and drag forces, respectively, and are considered the foremost parameters for comprehending the aerodynamic performance of an airfoil. The coefficient of lift (C_L), as defined by Eqn. (1), is a dimensionless parameter derived from the lift force (F_L), density (ρ), wind speed (V), and chord length (c). Similarly, the drag coefficient (C_D), which is determined using Eqn. (2), is a dimensionless quantity that represents the drag force F_D . The chord length is the distance between the trailing edge and the leading edge of an airfoil. Another crucial element in Eqn. (3) is the pressure coefficient (C_p), where the pressure difference is denoted by ΔP . The relative pressure throughout a flow field is indicated by the pressure coefficient C_p shown in Eqn. (3).

$$C_L = \frac{F_L}{\frac{1}{2}\rho V^2 c} \quad (1)$$

$$C_D = \frac{F_D}{\frac{1}{2}\rho V^2 c} \quad (2)$$

$$C_p = \frac{\Delta P}{\frac{1}{2}\rho V^2} \quad (3)$$

CFD Domain Description

A C-type domain was used in this study shown in Fig. 1(b), where the radius of the semicircle was 10 m, and the length of the rectangle was 20 m.

1000 mm chord model of the NACA 6309 airfoil was simulated using 100 coordinate points. The family of NACA airfoils is denoted by NACAYYXX where the first digit is meant to represent the percentage of maximum camber, the second digit represents the location of maximum camber from the leading edge in tenths of the chord and the last two digits represent the percentage of maximum thickness to chord. The airfoil was generated using the following equation:

$$y_t = 5t \left[0.2969 \sqrt{\frac{x}{c}} - 0.1260 \left(\frac{x}{c} \right) - 0.3516 \left(\frac{x}{c} \right)^2 + 0.2843 \left(\frac{x}{c} \right)^3 - 0.1015 \left(\frac{x}{c} \right)^4 \right] \quad (4)$$

Where c is the chord length, x is the position along the chord from 0 to c , y_t is the half thickness at a given value of x (center-line to surface), and t is the maximum thickness as a fraction of the chord.

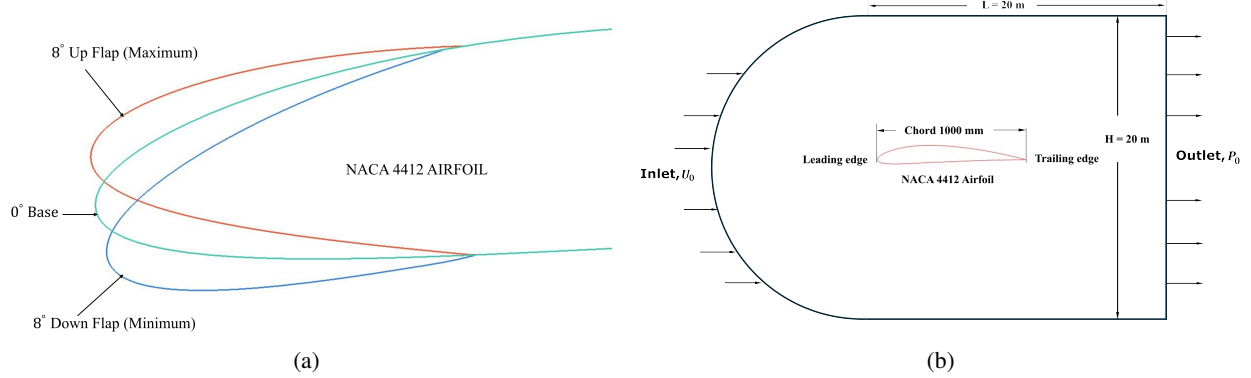


FIGURE 1. Schematic of (a) NACA 4412 airfoil with leading-edge 8° up flap and 8° down flap configuration and (b) C-type computational domain.

Governing Equations

Computational fluid dynamics (CFD) is the most widely used and accepted technique for performance analysis of airfoils. ANSYS FLUENT is one of the most reliable CFD facilities to simulate this kind of situation. CFD is based upon the Navier-Stokes equation which describes all kinds of partial fluids. The fundamental concept behind this equation is the conservation of mass, momentum, and energy. Eqn. (5) and Eqn. (6) represent the conservation of mass and momentum equation respectively.

$$\frac{\partial \rho}{\partial t} + \nabla \cdot (\rho \vec{V}) = S_M \quad (5)$$

$$\frac{\partial}{\partial t} (\rho \vec{V}) + \nabla \cdot (\rho \vec{V} \vec{V}) = -\nabla p + \nabla \cdot (\bar{\vec{r}}) + \rho \vec{g} + \vec{F} \quad (6)$$

$$\bar{\vec{r}} = \mu \left[(\nabla \vec{V} + \nabla \vec{V}^T) - \frac{2}{3} \nabla \cdot \vec{V} I \right] \quad (7)$$

In Eqn. (5), \vec{V} is a velocity vector and S_M is the source term. In Eqn. (6), P is the static pressure, while $\rho \vec{g}$ and \vec{F} , respectively, are the gravitational body force and the external body force. Additionally, in Eqn. (7), $\bar{\vec{r}}$ denotes the stress tensor. Since the direct numerical solution of this equation is extremely expensive and time-consuming, we had to select a turbulence model to execute this simulation. A single-equation model specifically created for aerospace applications is the Spalart-Almaras model. This model is used to solve a modeled transport equation for kinematic eddy viscosity [15]. In this model, the variable \tilde{v} is thought to be unaffected by the potent viscous effects.

$$\frac{\partial \tilde{v}}{\partial t} + \frac{\partial}{\partial t} (\rho \tilde{v} u_i) = G_v + \frac{1}{\sigma_{\tilde{v}}} \left[\frac{\partial}{\partial x_j} \left\{ (\mu + \rho \tilde{v}) \frac{\partial \tilde{v}}{\partial x_j} \right\} + C_{b2} \rho \left(\frac{\partial \tilde{v}}{\partial x_j} \right)^2 \right] - Y_v + S_{\tilde{v}} \quad (8)$$

In this Eqn. (8) Y_v stands for the destruction term and G_v represents the production of turbulent viscosity. Other elements that are used in this procedure are constant.

Grid Generation and Grid Sensitivity Analysis

The structured grid was constructed using ANSYS ICEM CFD. To capture the velocity gradient near the airfoil wall properly first layer thickness was estimated using the Reynolds number where $y+$ value kept less than unity

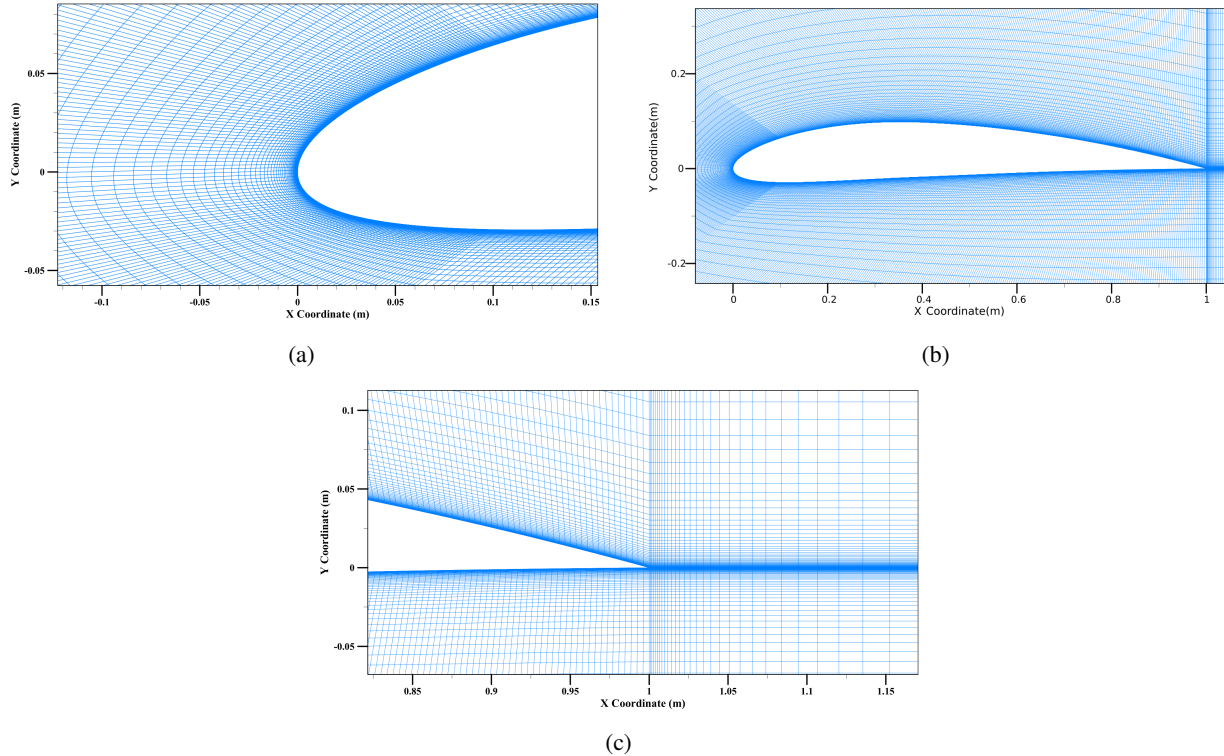


FIGURE 2. Structured mesh of C-type computational domain constructed using ANSYS ICEM CFD, (a) Airfoil, (b) Leading edge, and (c) Trailing edge.

($y+ < 1$). The detailed mesh around the leading and trailing edges is shown in Fig. 2(a) and Fig. 2(c), respectively, with the mesh around the airfoil domain depicted in Fig. 2(b).

Grid sensitivity analysis was conducted with element counts ranging from 68,805 to 251,155, as indicated in Table 1. The analysis revealed that the C_L/CD ratio increases up to 225,112 elements. Beyond this point, the variation is less than 1%. Hence, a total of 225,112 elements were chosen, along with a corresponding total of 223,980 nodes.

TABLE 1. Grid sensitivity analysis

Element Number	C_L/CD	Deviation, %
68,805	38.9986	-
111,800	45.5541	14.391 %
163,155	47.0654	3.2109 %
207,900	48.4584	2.8746 %
225112	48.5239	0.1351%
251,155	48.5314	0.0155%

Boundary Condition

Boundary conditions have to be faultless in order to obtain the proper output. At the inlet boundary, velocity inlet condition was applied with velocity magnitude and direction according to the angle of attacks from 0° to 20° . Velocity magnitude was constant and calculated from Re number at 0.3 million. At the outlet pressure outlet condition was applied. At the airfoil surface, no-slip condition was applied. In Table 2, initial boundary conditions of the CFD analysis. are provided.

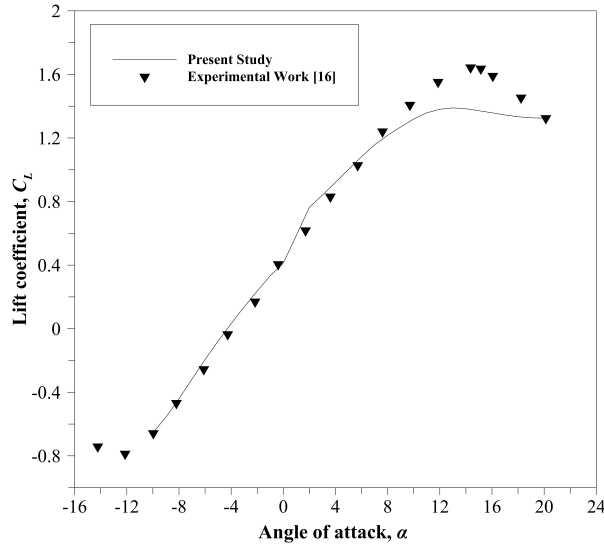


FIGURE 3. Validation of the present study with experimental work [16] for the coefficient of lift.

TABLE 2. Initial boundary conditions of the CFD analysis.

Simulation Property	Parameters	Solver Type	Time	Viscous Model	Number of Iterations	Momentum	Pressure Velocity Coupling
Fluid Property	Parameters	Fluid	Density (kg/m ³)	Viscosity (Ns/m ²)	Angle of Attack	Reynold Number	Pressure
	Value	Pressure based	Steady	Spalart-Allmaras	Close to 300	Second-order upwind	Simple
	Value	Air	1.225	1.7894	0° to 20°	300000	1 atm

Validation of CFD Model

Validation is crucial for any numerical investigation in order to measure accuracy and agreement with physical behaviour. In this study coefficient of lift (C_L) was validated with an experimental work conducted by NASA. It has been found that error between experimental and present study was 1.2 % and the agreement and accuracy of present study with experimental result is confirmed. Fig. 3 shows the comparison of the present study with naca 824 report [16] for NACA 4412 airfoil.

RESULT AND DISCUSSION

In order to determine the best and worst-performing airfoils configuration, the results of NACA 4412 airfoil considering leading edge flaps at 20% chord length under various angles of attack (0° to 20°) are reported in this section. The behavior between the airfoil's performance and the angle of attack is initially studied in relation to a critical parameter, the coefficient of lift. The second parameter to be addressed is the drag coefficient, which is also of significant importance. Additionally, the lift-to-drag ratio is analyzed to obtain which flap angle of NACA 4412 airfoil exhibits the highest and lowest performance. Following that, in an effort to pinpoint the underlying cause of such performance, static pressure contours are analyzed to understand the physics clearly. The distribution of static pressure contours and velocity contours surrounding the airfoils are then shown for the 8° up flap and down flap, respectively, to visualize the flow physics and understand the performance variations.

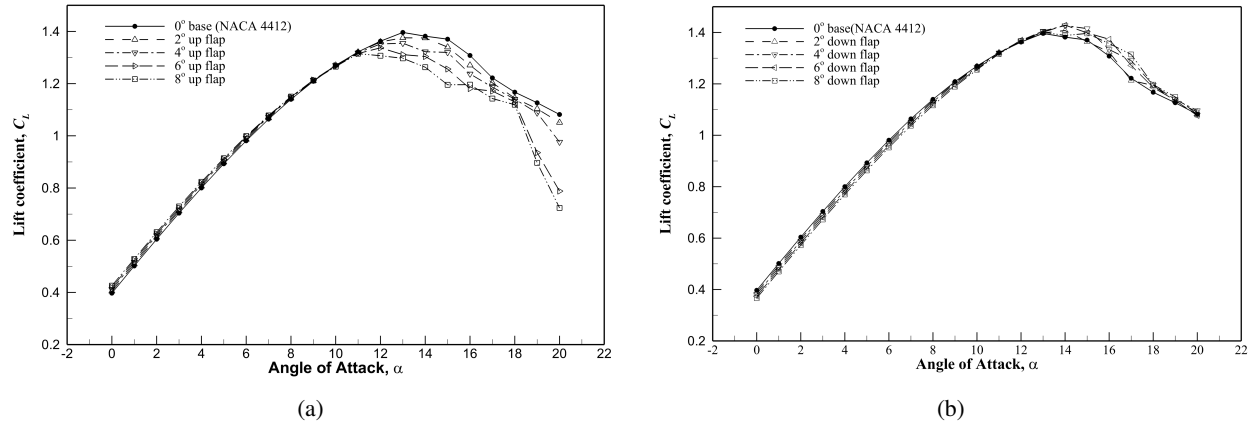


FIGURE 4. For AOA 0° to 20° , the variation of lift coefficient, (C_L) for (a) leading edge up flap and (b) leading edge down flap.

Characteristics of Coefficient of Lift

The angle of attack (α) significantly affects the lift and drag coefficient exerted on the airfoil. Our investigation reveals that the coefficient of lift typically increases up to a specific angle of attack. Beyond this angle, the coefficient of lift C_L starts to decrease until it reaches 20° AOA. The specific angle being referred to is known as the stall angle, which is the angle of attack at which the coefficient of lift reaches its highest value. For nearly all cases in our analysis, the stall angle spans between 12° and 14° .

When there is no leading-edge flap considered (0° flap), investigation shows that the value of the C_L is 0.39581 at 0° AOA. This value is enhanced until it reaches 14° . The highest value at the stall angle for this circumstance is 1.3892 at a 14° AOA. The coefficient of lift starts to diminish after crossing this stage, reaching a value of 1.0989 at a 20° angle of attack. The trend is nearly the same when the leading edge flap is taken into account.

Figure 4(a) shows that, in the range of 0° to 10° angle of attack, the coefficient of lift C_L is higher for every configuration of the leading edge up flap compared to the base (0° flap) configuration of the NACA 4412. Lift coefficient C_L falls under the base configuration of NACA 4412 after 10° angle of attack. The lift coefficient trend reveals the maximum and minimal offsets from the NACA 4412 base airfoil when employing the 8° up and 2° up flap configurations respectively, in contrast to all up-flap configurations. The highest and lowest coefficient of lift at the stall angle of 14° among the up-flap configurations is found to be 1.3749 and 1.2628 for 2° and 8° respectively. The highest coefficient of lift at the range of 0° angle 10° angle of attacks is found to be 1.2703 for 2° up flap which is considered as best configuration.

In the case of the leading edge down flap shown in Fig. 4(b), the coefficient of lift (C_L) is lower than the base (0° flap) configuration of NACA 4412 for the range of 0° to 12° angle of attack. Once the angle of attack reaches 12 degrees, the lift coefficient starts to exceed the value of the base configuration of NACA 4412. The highest and lowest coefficient of lift at the stall angle of 14° among the down flap configurations is found to be 1.4285 and 1.3880 for 6° and 8° down flap respectively. The 6° down flap is considered as best and 8° down flap is considered as worst.

In contrast 2° up flap is obtained optimum for a range of 0° angle 10° angle of attacks and 6° up optimum for 10° to 20° AOA.

Characteristics of Coefficient of Drag

While the airfoil's lift coefficient provides some insight into its overall performance, a comprehensive understanding can be obtained by analyzing the drag coefficient. For each configuration examined in our investigation, the drag coefficient consistently falls below acceptable thresholds and negligible deviation from the NACA 4412 base airfoil when the angle of attack (AOA) ranges from 0° to 14° or 15° . Also, the gradient of the C_D is very gradual in this range. Further increment of AOA results in a significant and rapid increase of C_D . At an AOA of 0° , when the leading-edge flap of the NACA 4412 airfoil is reduced to 0° the C_D is measured to be 0.0145. While the value of this C_D increases steadily up to an AOA of 15° , a significant increase is observed beyond this limit. The value increases from 0.059 at

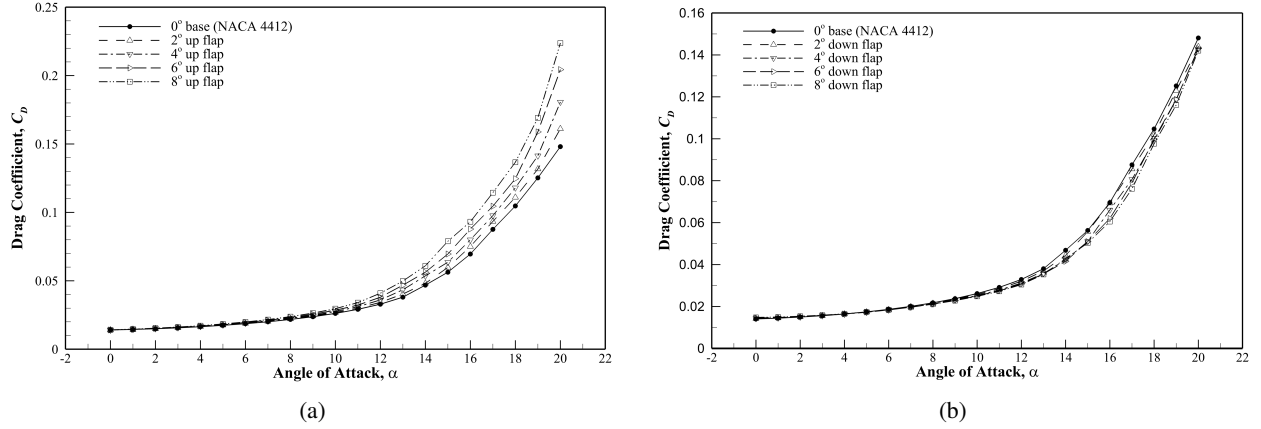


FIGURE 5. For AOA 0° to 20°, the variation of drag coefficient, (C_D) for (a) leading edge up flap and (b) leading edge down flap.

15° AOA to 0.073 at 16° AOA, demonstrating a substantial increment. This increment is continued until it reaches 20° AOA.

Figure 5(a) demonstrates that all up-flap configurations yield higher C_D in comparison to the NACA4412 base airfoil. After an angle of attack (AOA) of 10°, the deviation from the base airfoil progressively increases as the flap angle increases. The maximum and minimum deviation observed was approximately 51.1% for an 8° up flap and 2.52% for a 2° up flap at AOA of 20° respectively. The average deviation measure for an 8° up flap is 30.63%, whereas for a 2° up flap, it is 5.39 %. This suggests that all up-flap configuration is the worst-case scenario in terms of drag coefficient.

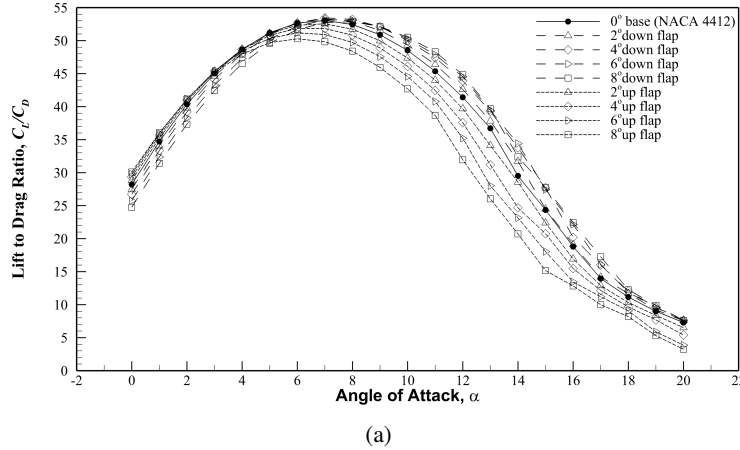
Figure 5(b) demonstrates that down flap configurations yield lower drag coefficients in comparison to the NACA 4412 base airfoil. After the angle of attack (AOA) of 10°, the deviation from the base airfoil gradually decreases as the flap angle increases downward. The maximum and minimum deviation observed was approximately 13.04% and 0.4% for an 8° down flap and 2° down flap respectively at AOA of 16°. The average deviation measure for an 8° down flap is +8.11%, whereas for a 2° down flap it is +2.33%. This positive percentile deviation represents the improvement in C_D and suggests that the 8° down flap is best in C_D .

Characteristics of Coefficient of Lift to Drag Ratio

Without a doubt, the most important parameter in determining optimal performance is the ratio of the coefficients of lift and drag (C_L/C_D). The optimal C_L/C_D versus AOA curve for the NACA 4412 airfoil is obtained at various leading edge flap angles and shown in Fig. 7. The NACA 4412 with 0° flap configuration, the C_L/C_D value is 28.20 at the 0° AOA. This trend continuously rises until the angle of attack reaches 7°. The highest value of C_L/C_D for all configurations is observed at this position; in the case of the base airfoil, it is 53.0623. However, after exceeding the 7° AOA, this value starts to diminish till 20°. At 20° AOA, the value of C_L/C_D is 7.30, which is the lowest in this case of a base airfoil.

Then when it comes to the leading-edge flap situation, the trend is nearly identical to the condition with no flap (0° flap). It is found that the down-flap configuration results in a higher C_L/C_D ratio, whereas the up-flap configuration yields a lower C_L/C_D ratio compared to the NACA 4412 base airfoil at all AOA. The maximum lift-to-drag ratio C_L/C_D was obtained to be 53.8 at the 8° down flap, while the minimum C_L/C_D was 49.8 with the 8° up flap at 7° AOA. The average deviation from NACA 4412 is determined to be -10.7% for an 8° down flap, indicating a significant enhancement in the C_L/C_D . On the contrary, the maximum average deviation compared to the NACA 4412 airfoil is determined to be +16.64% for an 8° up flap. This indicates that the performance of the up-flap airfoil is poorer than that of the NACA 4412.

Thus, the C_L/C_D exhibits significant enhancement when using the down flap configurations. The investigation revealed that the 8° down flap arrangement was the best flap configuration evaluated.



(a)

FIGURE 6. AOA 0° to 20° , the variation of lift to drag ratio (C_L/C_D) for leading edge up and down flap respectively.

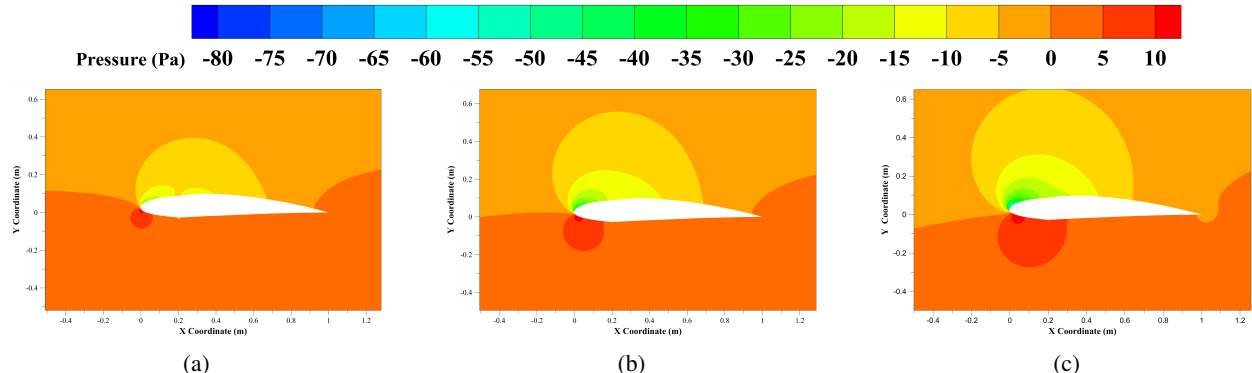
Investigation of Static Pressure

Any aerodynamic body's wings provide lift by developing more pressure at the lower than the upper parts of the body, providing a net upward force. Now, if the pressure below the airfoil rises due to a greater angle of attack, the net force rises, resulting in greater lift, but also greater total drag. Drag is developed when the pressure of the leading edge is greater than the pressure of the trailing edge of the airfoil. From the previous section, we have found the best and most performed airfoil, which is 8° down flap and 8° up flap at leading edge airfoil respectively. The following Fig. 7 and Fig. 8 demonstrate the static pressure contour of the NACA 4412 airfoil with an 8° up flap and 8° down flap respectively.

Intriguingly, it can be seen that the airfoil's pressure difference between the upper and lower edge increased with the increment of the AOA shown in Fig. 7 and Fig. 8 it can be seen that at 4° AOA pressure difference is lower and as AOA increased pressure difference also increased and at 12° it is much higher. Pressure difference maximum found between 12° - 14° AOA at which lift coefficient is highest. As AOA increases the pressure difference between the leading edge and trailing edge increases which indicate the increment of C_D with an increase of AOA.

In the case of the flap angle, it can be clearly understood by the contours that the up flap angle gives the highest pressure difference whereas for the down flap angle, the pressure difference is lower.

As seen from the contours 8° up flap gives 90 Pa of pressure difference and the 8° down flap gives 40 Pa overall pressure difference, which indicates that the 8° down flap gives a reduction in drag coefficient. From the pressure contour analysis, it is found that the 8° down flap is the best airfoil configuration and the 8° up flap is the worst.

**FIGURE 7.** Static Pressure Contour for NACA 4412 with 8° up flap at (a) 4° , (b) 8° , and (c) 12° angle of attack (α).

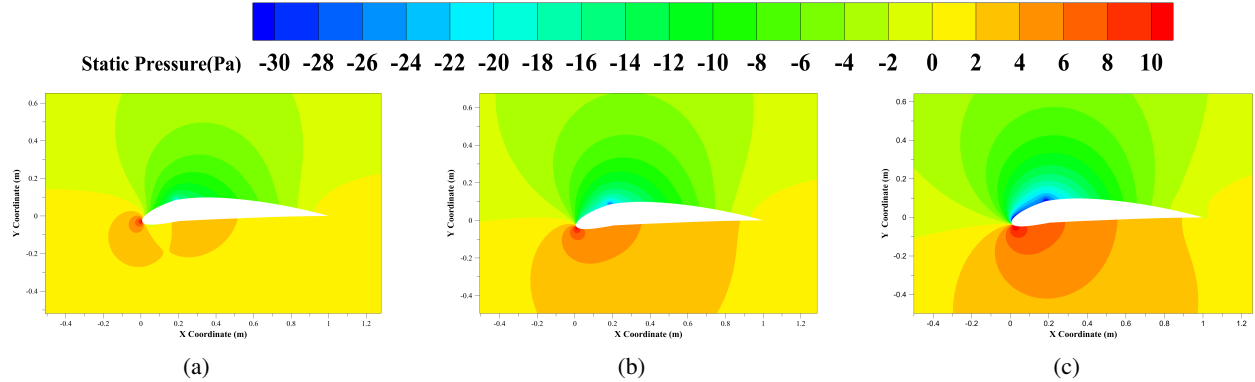


FIGURE 8. Pressure contour for NACA 4412 with 8° down flap at (a) 4°, (b) 8°, and (c) 12° angle of attack (α).

Investigation of Velocity Distribution

The velocity distribution surrounding the airfoil is depicted in Fig. 9 for the 8° up flap and Fig. 10 for the 8° down flap, where the AOA varies. As opposed to an 8° up flap, it is revealed that the 8° down flap has a greater velocity to the upper surface. Consequently, the 8° down flap produces a more substantial lift force due to the decreased pressure at the upper surface. Higher flow separation is noticed at the downstream for the 8° up flap as seen in the Fig. 9 indicating higher drag force.

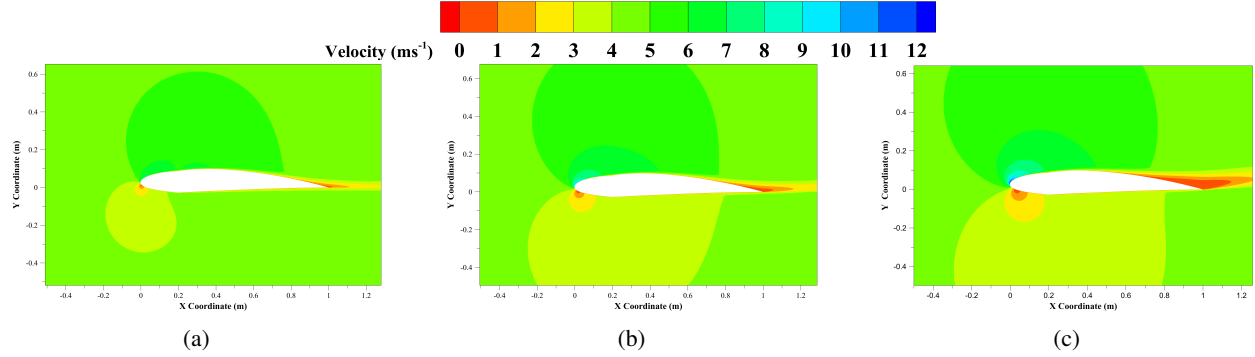


FIGURE 9. Velocity contour for NACA 4412 with 8° up flap at (a) 4°, (b) 8°, (c) 12° angle of attack (α).

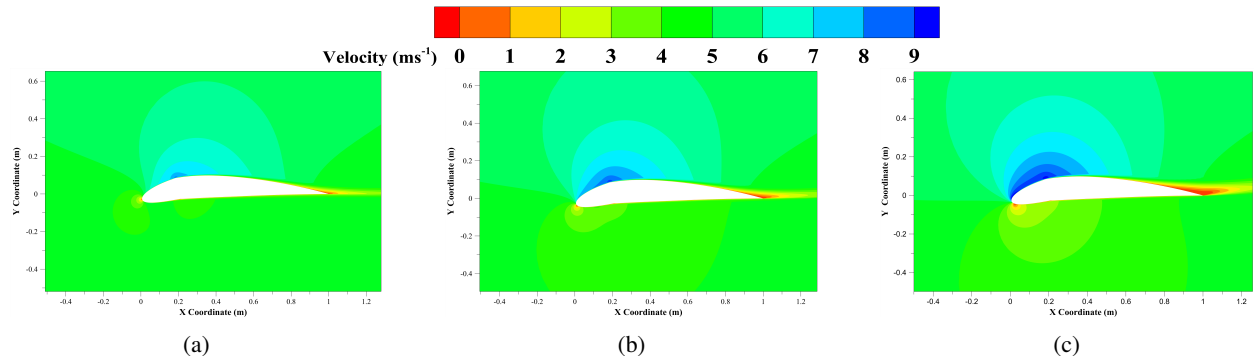


FIGURE 10. Velocity contour for NACA 4412 with 8° down flap at (a) 4°, (b) 8°, (c) 12° angle of attack (α).

CONCLUSION

The major focus of this study was to understand the impact of the leading-edge flap angle on the NACA 4412 airfoil. In this article, a variety of flaps on the leading edge are taken into account, and we then attempt to identify the ideal leading-edge flap that offers the highest performance among all flap configurations. For 0° to $\pm 8^\circ$ flaps at $Re = 0.3$ million with the Spalart-Allmaras turbulence model, the simulation is done with a 2° interval with a total of nine configurations. Finally, to recapitulate the research:

- The lift coefficient (C_L), drag coefficient (C_D), and lift coefficient-to-drag coefficient ratio (C_L/C_D) are found at different AOA for different leading edge flap conditions. Pressure and velocity distribution around the airfoils were analyzed to understand the flow physics.
- Almost every airfoil's C_L increases with the AOA up to 12° or 14° or the "stall angle," when the value of C_L is said to peak. The value of the C_L starts to decline after passing the stall angle. In the current investigation 2° up flap is obtained best for a range of 0° angle 10° AOA and 6° flap is best for 10° to 20° AOA.
- Every airfoil simulated in this study, experiences an increase in C_D as the AOA increases. When the AOA is close to 20° , the value of the C_D is much higher in every case, in spite of the fact that it grows slowly with the AOA at the initial level. In this study, the average deviation measured for an 8° down flap is $+8.11\%$, whereas for a 2° down flap, it is $+2.33\%$ with respect to NACA 4412 airfoil. In this study, 8° down flap performs best in terms of C_D . All up-flap airfoils perform poorer than NACA 4412 and are considered worst.
- In this study the lift coefficient-to-drag coefficient ratio (C_L/C_D) exhibits significant enhancement when using the down flap configurations. The investigation revealed that the 8° down flap arrangement was the best flap configuration evaluated. Maximum improvement was found in C_L/C_D is 10.7% for 8° down flap over the NACA 4412 base configuration. All up flaps perform lower than the NACA 4412 base configuration. The worst performance was observed with an 8° up flap which is 16.64% poorer than the NACA 4412 with no flap.

NACA 4412 with 8° down flap can be used in wind turbine applications. There is still various scope yet to study of the airfoil for investigation. Different parameters such as chord length, flap position, and operating conditions such as Reynolds number can be investigated to obtain optimum design for different locations.

REFERENCES

1. M. Zamani, M. J. Maghrebi, and S. R. Varedi, "Starting torque improvement using J-shaped straight-bladed Darrieus vertical axis wind turbine by means of numerical simulation," *Renewable Energy* **95**, 109–126 (2016).
2. P. Migliore, "Comparison of NACA 6-series and 4-digit airfoils for Darrieus wind turbines," *Journal of Energy* **7**, 291–292 (1983).
3. Şahin and A. Acir, "Numerical and Experimental Investigations of Lift and Drag Performances of NACA 0015 Wind Turbine Airfoil," *International Journal of Materials, Mechanics and Manufacturing* **3**, 22–25 (2015).
4. Z. Zhao, D. Wang, T. Wang, W. Shen, H. Liu, and M. Chen, "A review: Approaches for aerodynamic performance improvement of lift-type vertical axis wind turbine," *Sustainable Energy Technologies and Assessments* **49**, 101789 (2022).
5. Y. S. Rama Rao, M. V. N. Srujan Manohar, and S. V. V. Siva Praveen, "CFD simulation of NACA airfoils at various angles of attack," *IOP Conference Series: Materials Science and Engineering* **1168**, 012011 (2021).
6. I. Rabei, "Vertical Axis Wind Turbines: Open Airfoils and Plastic Blades," in *2021 International Conference on Electromechanical and Energy Systems (SIELMEN)* (IEEE, Iasi, Romania, 2021) pp. 051–056.
7. R. Jain and U. Mohammad, "Cfd approach of joukowski airfoil ($t= 12\%$), comparison of its aerodynamic performance with naca airfoils using k- ϵ turbulence model with 3 million reynolds number," *International Research Journal of Engineering and Technology* **5**, 1414–1418 (2018).
8. M. J. T. Loutun, D. H. Didane, M. F. Mohideen Batcha, K. Abdullah, M. F. Mohd Ali, A. N. Mohammed, and L. O. Afolabi, "2D CFD Simulation Study on the Performance of Various NACA Airfoils," *CFD Letters* **13**, 38–50 (2021).
9. A. E. S. L. J. V. D. Abbott, Ira H, "Summary of Airfoil Data," (1945).
10. P. Schubel and R. Crossley, "Wind Turbine Blade Design Review," *Wind Engineering* **36**, 365–388 (2012).
11. V. Khare, C. J. Khare, S. Nema, and P. Baredar, "Path towards sustainable energy development: Status of renewable energy in Indian subcontinent," *Cleaner Energy Systems* **3**, 100020 (2022).
12. J. Winslow, H. Otsuka, B. Govindarajan, and I. Chopra, "Basic understanding of airfoil characteristics at low reynolds numbers (10 4–10 5)," *Journal of aircraft* **55**, 1050–1061 (2018).
13. A. Mahato, R. K. Singh, R. Barnwal, and S. C. Rana, "Aerodynamic characteristics of naca 0012 vs. naca 4418 airfoil for wind turbine applications through cfd simulation," *Materials Today: Proceedings* (2023).
14. Q. Wang, J. Wang, J. Chen, S. Luo, and J. Sun, "Aerodynamic shape optimized design for wind turbine blade using new airfoil series," *Journal of Mechanical Science and Technology* **29**, 2871–2882 (2015).
15. M. N. Kaya, A. R. Kok, and H. Kurt, "Comparison of aerodynamic performances of various airfoils from different airfoil families using cfd," *Wind and Structures* **32**, 239–248 (2021).
16. P. Spalart and S. Allmaras, "A one-equation turbulence model for aerodynamic flows," in *30th aerospace sciences meeting and exhibit* (1992) p. 439.